NASA Technical Memorandum 104473
AIAA-91-2443

Carbon Monoxide and Oxygen Combustion Experiments: A Demonstration of Mars In Situ Propellants

Diane L. Linne
Lewis Research Center
Cleveland, Ohio

Prepared for the
27th Joint Propulsion Conference
cosponsored by AIAA, SAE, ASME, and ASEE
Sacramento, California, June 24-27, 1991

NASA

CARBON MONOXIDE AND OXYGEN COMBUSTION EXPERIMENTS: A DEMONSTRATION OF MARS IN SITU PROPELLANTS

Diane L. Linne
National Aeronautics and Space Administration
Lewis Research Center
Cleveland, Ohio 44135

Abstract

The feasibility of using carbon monoxide and oxygen as rocket propellants was examined both experimentally and theoretically. The steady-state combustion of carbon monoxide and oxygen was demonstrated for the first time in a sub-scale rocket engine. Measurements of experimental characteristic velocity, vacuum specific impulse, and thrust coefficient efficiency were obtained over a mixture ratio range of 0.30 to 2.0 and at chamber pressures of 1070 and 530 kPa (155 and 77 psia). The theoretical performance of the propellant combination was studied parametrically over the same mixture ratio range. In addition to one-dimensional ideal performance predictions, various performance reduction mechanisms were also modeled, including finite-rate kinetic reactions, two-dimensional divergence effects, and viscous boundary layer effects.

Introduction

As currently envisioned, the Space Exploration Initiative (SEI) presents an ambitious plan of expanding human presence into the solar system. The ultimate goal of manned missions to Mars will impose heavy burdens on both financial resources and launch capabilities. Many new technologies have been proposed for the Mars portion of the SEI scenario which would offer significant reduction in both fiscal and launch vehicle requirements. One such proposed new technology is the use of indigenous space materials to produce propellants for the return trip from Mars.

The atmosphere of Mars is 95 percent carbon dioxide. Several detailed studies have defined a production system that would separate the carbon dioxide into carbon monoxide and oxygen, and then store the propellants at cryogenic temperatures (Refs. 1 to 4). Mission analyses have shown a potential for significant reductions in Earth launch mass for both Mars precursor missions and for the manned Mars missions (Refs. 5,6). These analyses have been based on theoretically calculated values for combustion performance of a carbon monoxide and oxygen engine system. Before the use of in situ propellants can be planned into the SEI mission architectures, experimental testing and more rigorous theoretical performance predictions will be needed.

Some parametric calculations have been conducted for the performance of a carbon monoxide and oxygen rocket engine as a function of mixture ratio, chamber pressure, and nozzle area ratio (Refs. 7,8). These parametric studies have all used one-dimensional chemical equilibrium assumptions such as those in the CEC computer code (Ref. 9). Some mission analysts have reduced these predicted specific impulses by arbitrary amounts to account for the various performance losses inherent in a rocket engine.

The ignition characteristics of carbon monoxide and oxygen in a spark torch igniter have been evaluated experimentally (Ref. 10). The ignition boundaries as a function of mixture ratio and percent hydrogen in the carbon monoxide were established.

No experimental programs studying CO/O_2 combustion in a rocket engine have been performed prior to this study.

This paper discusses both theoretical predictions and experimental results for carbon monoxide and oxygen combustion in a rocket engine. Theoretically predicted performance losses caused by finite rate kinetics, two-dimensional geometry, and boundary layer effects are examined. Experimental results are presented as a demonstration of steady-state combustion, and are compared to the theoretical predictions.

Description of Computer Code

The Liquid Propellant Program (LPP) computer code (Ref. 11) was used for most of the theoretical predictions. This code uses a chamber and nozzle geometry together with thermodynamics and kinetics to predict the various performance losses that an actual engine will experience in normal operation. The code consists of several modules, each of which models a different type of performance loss. These modules are One-Dimensional Equilibrium (ODE), One-Dimensional Kinetics (ODK), Two Dimensional Kinetics (TDK), and Mass Addition Boundary Layer (MABL). All modules assume complete combustion in the chamber, that is, no loss in energy release due to slow vaporization or nonuniform mixing.

The ODE module predicts the ideal engine performance for an input pressure and enthalpy. The calculations are performed using the minimum-free-energy methodology. Performance is calculated based on equilibrium chemistry (i.e., infinite reaction rates). The ODK module predicts the inviscid, one-dimensional expansion of the gaseous combustion products through the converging-diverging nozzle. Equilibrium chemistry is assumed in the chamber and finite-rate kinetic chemistry is assumed in the nozzle.

The TDK module predicts the inviscid, two-dimensional expansion of the gaseous combustion products. A finite-difference mesh comprised of left running characteristics and streamlines is used to model the divergence losses in the nozzle. The initial line for the calculations is generated in a transonic flow module using the output from ODK. As in the ODK module, finite-rate kinetic chemistry is assumed in the nozzle.

The MABL module is a boundary layer module that models the growth of the viscous boundary layer in the chamber and nozzle. Because the test hardware was a small, low pressure engine, frozen chemistry was used to generate the necessary gas properties tables. To simulate the expected wall conditions, an estimated wall temperature profile was input based on knowledge of heat flux profiles in rocket engines and known operational limits of the engine material. For the theoretical analyses presented in this paper, MABL calculates the displacement thickness for the actual chamber and nozzle geometry and uses this to obtain a displaced, or inviscid, wall contour. The TDK module is then rerun with the new contour. A new mass flow rate is obtained by integrating the new initial line. This mass flow is then used in the calculation of characteristic velocity, C*, along with the actual or geometric throat area, to obtain a theoretical value of C*. These values are referred to as TDK/MABL predictions in the rest of this study to indicate that the TDK module was rerun with the displaced wall predicted by the boundary layer module.

Theoretical Analysis

Several mission analyses have been performed recently that have investigated the potential benefits

of using carbon monoxide and oxygen produced at Mars for portions of a round trip mission (Refs. 5,6). Most of these missions have assumed a specific impulse of 260 to 280 sec for the expected performance of this propellant combination. In this range of specific impulse, a 10 sec change in delivered performance can significantly affect the results of the mission analysis. A parametric evaluation was performed to determine the expected performance of carbon monoxide and oxygen.

One-Dimensional Equilibrium

A one-dimensional equilibrium computer code (Ref. 9) was used to calculate vacuum specific impulse as a function of mixture ratio, chamber pressure, and area ratio. Figure 1 shows the results of this parametric study for a mixture ratio range of 0.25 to 2.0, chamber pressures of 1.4 and 20.7 MPa (200 and 3000 psia), and area ratios of 10, 60, 100, 200, and 500. The curves exhibit typical liquid rocket engine behavior, with peak specific impulse occurring between a mixture ratio of 0.40 and 0.60 (stoichiometric mixture ratio is 0.571). As expected, chamber pressure has a small effect on specific impulse, with only a 5 or 6 sec increase in specific impulse gained with an increase in chamber pressure from 1.4 to 20.7 MPa.

The figure shows that theoretical specific impulses as high as 313 sec are predicted for a low pressure engine with a nozzle expansion ratio of 500. These higher predicted specific impulses could have a significant effect on the results of the mission analyses that assumed only a 260 to 280 sec specific impulse. The 313 sec, however, is an ideal theoretical prediction, and an actual engine would not be expected to deliver this performance. To predict the performance losses that may occur with the operation of an actual engine, a second computer code was used to predict performance losses associated with finite-rate kinetics, two-dimensional flow, and boundary layer growth.

Predicted Performance Losses

To predict performance losses, the LPP computer code requires that an engine geometry be specified. The required parameters include chamber radius and length, throat radius, upstream and downstream radius of curvature at the throat, nozzle contour, and nozzle inlet and outlet angles. Because no CO/O_2 rocket engine has been designed to date, the geometry from an RL10 rocket engine was used for this part of the analysis. This version of the RL10 has a throat radius of 6.53 cm (2.57 in.), an expansion ratio of 205, and is regeneratively cooled with hydrogen to an area ratio of 60. For the CO/O_2 analysis, a chamber pressure of 1.4 MPa (200 psia) was assumed, and liquid carbon monoxide was used as a coolant (Ref. 8). Liquid oxygen is also a viable option as a coolant for a carbon monoxide/oxygen engine.

Figure 2 shows the predicted vacuum specific impulse for the carbon monoxide/oxygen propellant combination as a function of mixture ratio. The four lines represent the performance predicted by the various modules of the computer code; they represent the different types of performance losses that are obtained in an actual engine. The top line (ODE) in the figure represents the ideal, one-dimensional equilibrium performance; these values are the same as those in Fig. 1 for an area ratio of 200 and a chamber pressure of 1.4 MPa (200 psia). The second line (ODK) in the figure represents the one-dimensional performance with finite-rate kinetics assumed instead of chemical equilibrium. The third line (TDK) in the figure adds two-dimensional flow losses. Finally, the fourth line (TDK/MABL) in the figure represents the predicted

performance with the effects of boundary layer growth also included.

For the conditions modeled here, significant performance losses are predicted, and the ideal specific impulse of nearly 305 sec is reduced to 260 sec. Figure 3 shows the specific impulse efficiency predicted by the various computer modules. These values were obtained by dividing the predicted specific impulse by the ideal values from the ODE module. The figure shows a significant decline in efficiency as the stoichiometric mixture ratio of 0.571 is approached.

It can be seen from Figs. 2 and 3 that the largest losses occur when finite-rate kinetics are included in the calculations. These losses are caused by the high rate of dissociation of the carbon dioxide and the slow rate of recombination. Figure 4 shows the mole fraction of carbon dioxide for different locations in the engine, as indicated by area ratio. Both ODE and ODK predictions are shown for three chamber pressures at a mixture ratio of 0.55. This graph illustrates several chemical reaction patterns. First, most recombination occurs very close to the throat area. Recombination begins upstream of the throat when the temperature begins to drop and shifts the equilibrium constant. Recombination ends shortly downstream of the throat when the temperature becomes too low for further reaction. Because the ODK module considers finite reaction rates, it does not predict as much recombination as the ODE module with its assumption of infinite reaction rates.

Second, the figure clearly shows that at higher pressures, there is less dissociation in the chamber. This in itself will give a higher predicted performance, as was seen in Fig. 1. Finally, the figure shows that more recombination is predicted in the ODK modules at higher chamber pressures. As chamber pressure increases, gas density also increases, and species production increases. The low ODK efficiency shown in Fig. 3, therefore, is caused by the low rate of recombination at the low chamber pressure.

The ODE and ODK calculations were rerun over the entire mixture ratio range at a chamber pressure of 20.7 MPa (3000 psia), and much higher ODK efficiencies were obtained. Figure 5 shows the ODK efficiencies obtained at the two different chamber pressures. The increase in chamber pressure reduces the predicted kinetic losses at the stoichiometric mixture ratio from greater than 8 percent to a little more than 3 percent. This figure shows that although chamber pressure had a negligible effect on predicted ideal specific impulse (Fig. 1), it can have a significant effect on actual specific impulse.

The results of the theoretical predictions of the performance losses made by the LPP computer code indicate that slow recombination rates could cause significant reductions in delivered specific impulse at low chamber pressures. To compare actual engine performance with the theoretical predictions, an experimental program was conducted to measure the performance of a low-pressure carbon monoxide/oxygen rocket engine.

Test Apparatus and Procedure

Test Facility

The experimental tests for this study were performed in Cell 21 of the Rocket Lab at the NASA Lewis Research Center. This facility contains a low thrust rocket engine test stand with supporting fluid systems that allow precise flow of several fuel and oxidizer combinations. Four separate propellant lines were used for this research program: one oxygen supply line (primary) to the

engine, one oxygen supply line (secondary) to the spark torch igniter, one carbon monoxide fuel supply line to the engine, and one hydrogen fuel supply line to the igniter.

The flow rate of each of the gases in the system described above was controlled with a sonic orifice. Inserted as a component of the propellant line, each orifice insured a constant flow rate of gas, independent of downstream pressure perturbations. By measuring the line pressure and temperature at a point just upstream of each sonic orifice, and using orifice calibration curves, gas flow rates were calculated. Different diameter orifices could be easily interchanged in the system so that the gas flow rate range could be varied throughout the test program. The primary oxygen flow rate ranged from 10.9 to 68.0 g/sec (0.024 to 0.150 lbm/sec). The carbon monoxide flow rate ranged from 16.8 to 75.6 g/sec (0.037 to 0.160 lbm/sec). The total flow rate was held relatively constant at 47.5 and 95.3 g/sec (0.105 and 0.210 lbm/sec). ODE predicted chamber pressures for these two total flow rates are 520 and 1240 kPa, respectively (90 and 180 psia). Actual chamber pressures achieved were approximately 530 and 1070 kPa (77 and 155 psia).

Test Hardware

The test hardware for this experiment consisted of standard liquid rocket engine hardware including an igniter, injector, chamber spool piece, and converging-diverging nozzle. Figure 6 shows a schematic of the assembled engine, the injector face, and an injector element.

A hydrogen-oxygen spark torch igniter was used to initiate combustion. Gaseous oxygen and gaseous hydrogen were injected into the igniter chamber at an oxygen-to-fuel mixture ratio (O/F) of approximately 40, where a standard spark plug initiated combustion. The hot gases then travelled down a tube through the injector manifolding and into the combustion chamber. At the exit of the igniter tube, additional gaseous hydrogen, which had been used to cool the outside of the igniter tube, was added to the hot gases to increase the flame temperature. The total igniter mixture ratio at the exit of the igniter tube was approximately 7.5.

An eight element triplet injector design was used to inject the primary propellants into the combustion chamber. Each triplet element was a fuel-oxygen-fuel (F-O-F) design. The eight elements were arranged in a mutually perpendicular manner surrounding the igniter outlet orifice to promote inter-element mixing. The two outer orifices had an impingement angle of 50° (inclusive). Because the pressure and density of the gases will vary rapidly as mass flow rates change, two injectors were used to cover the desired mixture ratio range of 0.30 to 2.0. Injector 1 was used for mixture ratios of 0.30 to 0.80, and injector 2 was used for mixture ratios of 0.90 to 2.0.

A copper heat sink chamber and nozzle were used. The chamber had an interior diameter of 5.22 cm (2.055 in.), and was 20.3 cm (8 in.) long. A chamber pressure tap was located at the entrance of the chamber next to the injector. The nozzle had a throat diameter of 1.15 cm (0.454 in.), and an exit area ratio of 2.363. The diverging nozzle contour was a cone, with an exit half-angle of 15°. Figure 7 shows the engine mounted on the thrust rig during a test.

Test Procedure

To insure a uniform run profile throughout the duration of the test program, each firing of the igniter

was sequenced by a programmable line controller. Each test run started with the initiation of the secondary oxygen and the hydrogen flows to the igniter and the primary oxygen flow to the engine. One tenth of a second later, the spark was started, followed one tenth of a second after that by the carbon monoxide, at which point the main combustion was initiated. After combustion started, the secondary oxygen and the hydrogen to the igniter were stopped, and the test continued for 1.2 sec with no hydrogen flowing. This sequencing allowed for hydrogen to be present during ignition of the engine to aid in the ignition of the dry carbon monoxide and oxygen mixture (Ref. 10). The steady-state portion of the test run from which the data was taken, however, was after the hydrogen flow had been terminated, demonstrating steady-state combustion of dry carbon monoxide and oxygen.

Experimental data was gathered during the test runs by a high-speed data acquisition system. In addition to the instrumentation on the hardware, pressure transducers and thermocouples were applied to the facility feed systems to properly measure the propellant flow rates and temperatures. A total of 100 instrumentation channels were scanned at the rate of 100 times per second per channel. For each channel, every ten readings were combined to provide approximately ten averaged data points per second. All values quoted in this analysis were obtained by averaging together three of these averaged data points. Therefore, each value quoted is an average of 30 readings of the instrument by the data system. The data reduction was performed by a FORTRAN 77 computer program hosted on a VAX cluster.

Experimental Results

Two measures of engine performance were taken during the experimental tests. The first was characteristic velocity, C*, which was calculated based on the measured chamber pressure and propellant flow rates. The second measure of performance was the vacuum specific impulse, which was calculated based on the measured propellant flow rates and measured thrust corrected to vacuum conditions by adding the nozzle exit pressure force. Both of these performance measurements were compared to theoretical values predicted by the LPP computer code.

Some of the experimental results are tabulated in Appendix A. For each of the two chamber pressures, three tests were performed at each mixture ratio. Only one test at each mixture ratio is shown in the tables as a representative value.

Figure 8 shows the experimental and theoretical values of characteristic velocity for two chamber pressures over a range of mixture ratios. As seen before, the chamber pressure has little effect on the theoretical predicted C*. For the experimental results, different symbols are used to denote results from the two different injectors. As can be seen in the figure, a discontinuity exists where the injectors were changed. Table 1 lists some of the operating characteristics of the injectors. Pressure drop as a percent of chamber pressure, injection velocities, velocity ratio, and momentum ratios are listed at each chamber pressure. Velocity and momentum ratios are calculated as fuel to oxidizer ratios. Each injector was designed for the midpoint of the mixture ratio range at which it would be used. Because the densities and pressures of the gases vary rapidly as mass flow rates change, the upper and lower end of each injector's operating range may produce nonoptimum injector performance. This was the cause of the discontinuity between mixture ratios of 0.80 and 0.90.

It can be seen in Fig. 8 that the experimental C* curve has the same general shape as the theoretical curve, but appears to peak at a higher mixture ratio and is significantly lower. To quantify the difference between experimental and predicted C*, the experimental values were divided by the one-dimensional equilibrium values, and C* efficiency was plotted in Fig.9. The theoretical efficiencies plotted are the TDK/MABL predicted values divided by the ODE values. The LPP code predicts C* efficiencies between 95 and 97 percent (note the increase in predicted efficiency with increased pressure). These theoretical efficiencies are much higher than those shown in the previous section because the expansion area ratio of the test hardware was only 2.4, and the predicted kinetic recombination rates are still close to the equilibrium values to this point. The experimental values fall between 89 and 93 percent. The theoretical predictions of C* efficiency account for expected performance losses caused by finite-rate kinetics, two-dimensional flow, and boundary layer growth. The LPP code, however, assumes complete combustion in the chamber. The difference between the theoretical and experimental C* efficiencies in Fig. 9, therefore, are most likely caused by incomplete energy release in the chamber. Because both propellants were gaseous, the most probable cause of incomplete energy release is poor mixing between the gases. A more optimum injector design would most likely increase the experimental efficiency toward the level predicted by the LPP computer code.

Experimental vacuum specific impulse was also measured, and is shown in Fig. 10 along with the ODE theoretical values. It should be noted that because the expansion area ratio of the experimental hardware was only 2.4 the actual magnitude of the specific impulse is not significant here. As in the figures of C*, the experimental I_{vac} curve has a similar shape to the theoretical curve. Figure 11 shows the experimental and theoretical vacuum specific impulse efficiencies as a function of mixture ratio. The theoretically predicted efficiencies are about 93 to 95 percent, while the experimental efficiencies are 85 to 89 percent. This difference is most likely caused by the incomplete energy release that was observed in the C* efficiency graph. In Fig. 9, the difference between the theoretical and experimental values of C* efficiency average 6 percent. If the theoretical vacuum specific impulse efficiencies in Fig. 11 are reduced by 6 percent to account for losses caused by incomplete energy release, then the theoretically predicted efficiency would be approximately 88 percent. This is right in line with the experimental values shown. Therefore, the difference in Fig. 11 between the theoretical and experimental curves is again probably caused by the incomplete energy release that the LPP computer code does not take into account.

Theoretical and experimental thrust coefficient efficiencies are graphed in Fig. 12. Thrust coefficient is dependent on the hardware geometry, and theoretical and experimental thrust coefficient efficiency should coincide. The theoretical and experimental values were obtained by dividing the TDK/MABL predicted values and the experimental values of thrust coefficient by the ODE predicted value. In Fig. 12, the experimental thrust coefficient efficiencies obtained with injector 1 at low pressure (530 kPa) coincide with the theoretical predictions. The experimental thrust coefficient efficiencies obtained with injector 2 at low pressure and with both injectors at high pressure (1070 kPa), however, are approximately 2 percent lower than theoretical predictions.

Reexamining Figs. 8 and 10, the experimental C* for the higher pressure (1070 kPa) is slightly higher than that for the lower pressure (530 kPa), agreeing with the theoretical predictions. In Fig. 10, however, the experimental specific impulse at the lower pressure is higher than that for the higher pressure for tests run with injector 1. Because the low pressure, injector 1 set of data is the only set that coincides with theoretical thrust coefficient efficiencies (Fig. 12), it is possible that a bias error was introduced for the remaining specific impulse measurements. An examination of the raw experimental data and the thrust stand calibration curves did not disclose any obvious source of this bias error.

Conclusion

An engine performance computer code was used to parametrically study the theoretical performance in a carbon monoxide/oxygen rocket engine. Losses caused by finite-rate kinetic reactions, two-dimensional flow effects, and boundary layer growth were calculated. At a chamber pressure of 1.4 MPa (200 psia) and an expansion area ratio of 205, the code predicted vacuum specific impulse reduction from ideal (ODE) of as much as 14 percent at a stoichiometric mixture ratio. More than 8 percent of these losses were caused by finite-rate kinetic reactions in the expanding nozzle. Further parametrics indicated that the kinetic losses were reduced to 3 percent if chamber pressure was increased to 20.7 MPa (3000 psia). This indicates that the high rate of dissociation of the carbon dioxide at the lower pressures was the main cause of the kinetic inefficiencies. The results of the theoretical analysis indicate that a specific impulse in the range of 260 to 280 sec is realistic for the assumption of a low pressure engine. Specific impulses of 290 to 300 sec should be used, however, for the assumption of a higher pressure, pump-fed engine.

Gaseous carbon monoxide and oxygen were combusted in a sub-scale rocket engine, demonstrating steady-state combustion of this potential Mars in situ propellant combination. C* and vacuum specific impulse efficiencies of 89 to 93 percent and 85 to 89 percent, respectively, were obtained from the experimental program. These experimental efficiencies are approximately 6 percent lower than the efficiencies predicted by the theoretical computer code for this specific test hardware. This discrepancy between the theoretical and experimental values is most likely caused by incomplete energy release in the chamber due to nonuniform mixing of the gases. The computer program results assume complete combustion in the chamber.

The results of the theoretical parametric studies and the experimental tests indicate that with careful engine design, a carbon monoxide/oxygen rocket engine can be developed to perform with reasonable efficiency. Such an engine will allow the use of in situ propellants for the return trip from Mars. This could significantly reduce the launch vehicle requirements of future manned Mars missions.

Appendix A

TABLE A1. - EXPERIMENTAL DATA FOR CO/O_2 COMBUSTION TESTS

(SEE BELOW FOR KEY TO COLUMN HEADINGS)

[P_c = 530 kPa (77 psia); Injector 1.]

Rdg (a)	O/F (b)	C^*_{th}, m/s (c)	C^*_x, m/s (d)	η_{C^*}, percent (e)	I_{vacth}, sec (f)	I_{vacx}, sec (g)	η_{Ivac}, percent (h)	C_{fth} (i)	C_{fx} (j)	η_{Cf}, percent (k)
123	0.304	1347	1198	89.0	207.4	180.3	86.9	1.510	1.476	97.7
124	.346	1355	1213	89.6	209.3	182.7	87.3	1.515	1.477	97.5
125	.405	1358	1223	90.1	210.1	184.4	87.8	1.517	1.478	97.4
126	.452	1359	1226	90.2	210.2	184.9	88.0	↓	1.479	97.5
127	.502	1358	1227	90.4	210.0	185.5	88.3	↓	1.482	97.7
128	.554	1356	↓	90.4	209.8	185.1	88.2	↓	1.480	97.6
129	.614	1353	↓	90.6	209.3	185.4	88.6	↓	1.482	97.7
130	.648	1351	↓	90.8	209.1	185.4	88.7	↓	1.482	97.7
131	.699	1349	1225	90.8	208.6	184.6	88.5	↓	1.477	97.4
132	.807	1342	1222	91.0	207.6	184.2	88.7	↓	1.479	97.5

[P_c = 530 kPa (77 psia); Injector 2.]

Rdg (a)	O/F (b)	C^*_{th}, m/s (c)	C^*_x, m/s (d)	η_{C^*}, percent (e)	I_{vacth}, sec (f)	I_{vacx}, sec (g)	η_{Ivac}, percent (h)	C_{fth} (i)	C_{fx} (j)	η_{Cf}, percent (k)
205	0.855	1338	1203	89.9	206.9	177.8	85.9	1.517	1.450	95.6
204	0.957	1331	1199	90.1	205.8	177.3	86.2	1.516	1.450	95.6
203	1.190	1315	1185	90.2	203.1	174.8	86.1	1.515	1.446	95.4
202	1.400	1298	1170	90.1	200.5	172.5	86.0	1.514	1.446	95.5
201	1.650	1279	1150	89.9	197.2	169.3	85.9	1.512	1.444	95.5
200	1.940	1255	1121	89.4	192.9	165.3	85.7	1.508	1.446	95.9

[P_c = 1070 kPa (155 psia); Injector 1.]

Rdg (a)	O/F (b)	C^*_{th}, m/s (c)	C^*_x, m/s (d)	η_{C^*}, percent (e)	I_{vacth}, sec (f)	I_{vacx}, sec (g)	η_{Ivac}, percent (h)	C_{fth} (i)	C_{fx} (j)	η_{Cf}, percent (k)
154	0.321	1358	1216	89.5	209.3	179.1	85.6	1.511	1.445	95.6
155	.373	1366	1230	90.0	211.1	181.0	85.7	1.515	1.444	95.3
156	.431	1369	1236	90.3	211.6	182.0	86.0	1.516	1.444	95.3
157	.481	1369	1238	90.4	211.6	182.5	86.2	1.516	1.446	95.4
158	.537	1367	1240	90.7	211.4	182.9	86.5	1.517	1.447	95.4
164	.593	1365	1246	91.3	211.1	183.5	86.9	1.517	1.444	95.2
163	.647	1362	1244	91.4	210.7	183.3	87.0	1.517	1.444	95.2
162	.681	1360	1243	91.4	210.3	183.2	87.1	1.516	1.445	95.3
161	.727	1358	1241	91.4	209.9	182.8	87.1	1.516	1.445	95.3
160	.836	1351	1232	91.2	208.8	181.8	87.1	1.516	1.447	95.4

[P_c = 1070 kPa (155 psia); Injector 2.]

Rdg (a)	O/F (b)	C^*_{th}, m/s (c)	C^*_x, m/s (d)	η_{C^*}, percent (e)	I_{vacth}, sec (f)	I_{vacx}, sec (g)	η_{Ivac}, percent (h)	C_{fth} (i)	C_{fx} (j)	η_{Cf}, percent (k)
187	0.908	1345	1242	92.3	207.9	181.5	87.3	1.516	1.433	94.5
186	1.000	1338	1237	92.4	206.8	180.5		1.516	1.431	94.4
185	1.210	1323	1221	92.3	204.3	178.4		1.515	1.432	94.5
184	1.460	1303	1201	92.2	200.9	175.4		1.512	1.432	94.7
183	1.710	1281	1180	92.1	197.2	172.1		1.510	1.430	94.7
182	1.890	1265	1160	91.7	194.4	169.3	87.1	1.508	1.432	95.0

[a] Rdg — Test reading number.
[b] O/F — Oxygen to fuel mixture ratio.
[c] C^*_{th} — Theoretical characteristic velocity.
[d] C^*_x — Experimental characteristic velocity.
[e] η_{C^*} — Characteristic velocity efficiency.
[f] I_{vacth} — Theoretical vacuum specific impulse.
[g] I_{vacx} — Experimental vacuum specific impulse.
[h] η_{Ivac} — Vacuum specific impulse efficiency.
[i] C_{fth} — Theoretical thrust coefficient.
[j] C_{fx} — Experimental thrust coefficient.
[k] η_{Cf} — Thrust coefficient efficiency.

References

1. Frisbee, R.H., "Mass and Power Estimates for Mars In Situ Propellant Production Systems," AIAA-87-1900, July, 1987.

2. Ash, R.L., Huang, J-K., Johnson, P.B., and Sivertson, W.E., "Elements of Oxygen Production Systems Using Martian Atmosphere," AIAA-86-1586, June, 1986.

3. Schallhorn, P., Colvin, J., and Ramohalli, K., "Propellant Production on Mars: Oxygen," AIAA-91-2444, June, 1991.

4. Hepp, A.F., Landis, G.A., and Linne, D.L., "Material Processing with Hydrogen and Carbon Monoxide on Mars," NASA TM-104405, May, 1991.

5. French, J.R., "Rocket Propellants from Martian Resources," Journal British Interplanetary Society, Vol. 42, pp. 167-170, 1989.

6. Stancati, M.L., Niehoff, J.C., and Wells, W.C., "Mars Automated Refueling System Final Report and Presentation," Report No. SAI 1-120-196-S7, October, 1978.

7. Clapp, W.M., "Propellant Performance of Mars-Produced Carbon Monoxide," AIAA-86-1587, June, 1986.

8. Armstrong, E.S., "Cooling of In Situ Propellant Rocket Engines for Mars Mission," NASA TM-103729, January, 1991.

9. Gordon, S., and McBride, B.J., "Computer Program for Calculation of Complex Chemical Equilibrium Compositions, Rocket Performance, Incident and Reflected Shocks, and Chapman-Jouguet Detonations," NASA SP-273, March, 1976.

10. Linne, D.L., Roncace, J., and Groth, M.F., "Mars In Situ Propellants: Carbon Monoxide and Oxygen Ignition Experiments," NASA TM-103202, AIAA-90-1894, July, 1990.

11. Nickerson, G.R., Coats, D.E., Dang, A.L., Dunn, S.S., and Kehtarnavaz, H., "Two-Dimensional Kinetics (TDK) Nozzle Performance Computer Program," NAS8-36863, March, 1989.

TABLE 1. - INJECTOR EXPERIMENTAL CHARACTERISTICS

[P_c = 1070 MPa (155 psia).]

Test rdg number	O/F	$\Delta P_{ox}/P_c$, percent	$\Delta P_f/P_c$, percent	V_{ox}, m/s	V_f, m/s	Velocity ratio	Momentum ratio
154	0.321	21.4	31.0	135	183	1.35	4.21
155	.373	26.6	28.2	148	175	1.18	3.16
156	.431	32.8	26.0	163	167	1.02	2.36
157	.481	38.5	24.4	175	161	0.920	1.91
158	.537	44.6	22.6	187	155	.829	1.55
164	.593	51.0	20.3	205	150	.731	1.23
163	.647	56.1	19.2	216	145	.671	1.04
162	.681	59.4	18.4	223	143	.639	0.942
161	.727	63.6	17.5	233	139	.598	.825
160	.836	74.9	15.8	252	132	.522	.625
187	.908	24.4	64.8	140	246	1.76	1.94
186	1.00	26.9	59.4	147	236	1.60	1.60
185	1.21	32.9	50.6	163	217	1.33	1.10
184	1.46	39.7	42.5	179	199	1.11	0.762
183	1.71	46.4	36.6	193	184	0.951	.557
182	1.89	51.2	33.6	204	176	.862	.457

[P_c = 530 kPa (77 psia).]

Test rdg number	O/F	$\Delta P_{ox}/P_c$, percent	$\Delta P_f/P_c$, percent	V_{ox}, m/s	V_f, m/s	Velocity ratio	Momentum ratio
123	0.304	21.4	38.1	141	202	1.43	4.71
124	.346	25.3	34.9	154	194	1.26	3.64
125	.405	31.5	32.0	171	184	1.08	2.66
126	.452	36.9	30.1	184	178	0.965	2.14
127	.502	42.5	28.3	197	172	.872	1.74
128	.554	48.6	26.8	210	166	.791	1.43
129	.614	55.3	24.9	224	160	.714	1.16
130	.648	59.0	24.1	231	157	.678	1.05
131	.699	64.0	22.0	242	152	.628	0.900
132	.807	77.0	20.8	263	144	.546	.677
205	.855	25.2	73.2	140	260	1.86	2.18
204	.957	28.0	66.1	148	248	1.67	1.75
203	1.19	35.7	54.6	166	225	1.36	1.14
202	1.40	41.9	46.8	180	208	1.16	0.823
201	1.65	49.4	40.0	195	192	0.986	.598
200	1.94	57.7	34.3	211	178	.844	.434

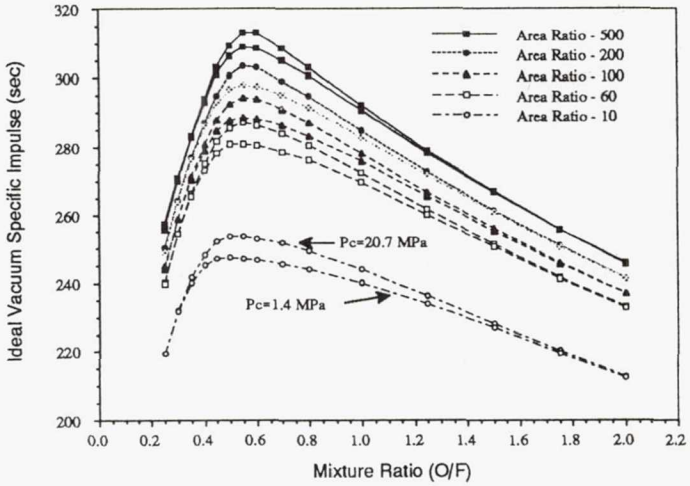

Figure 1. - One dimensional equilibrium specific impulse performance for LO2/LCO

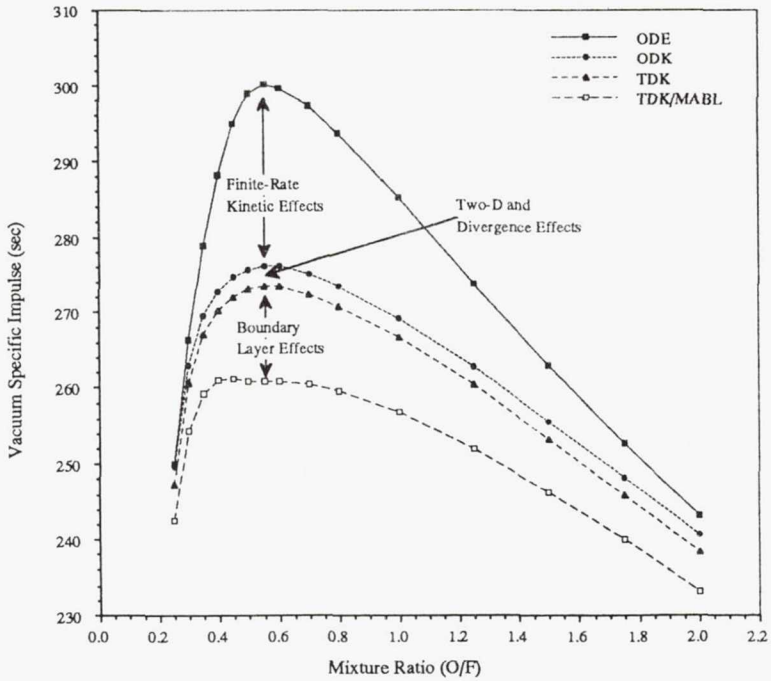

Figure 2. - Theoretical specific impulse performance for O2/CO in an RL10 rocket engine (Pc=1.4 MPa, Area Ratio=205, LCO regen. cooled)

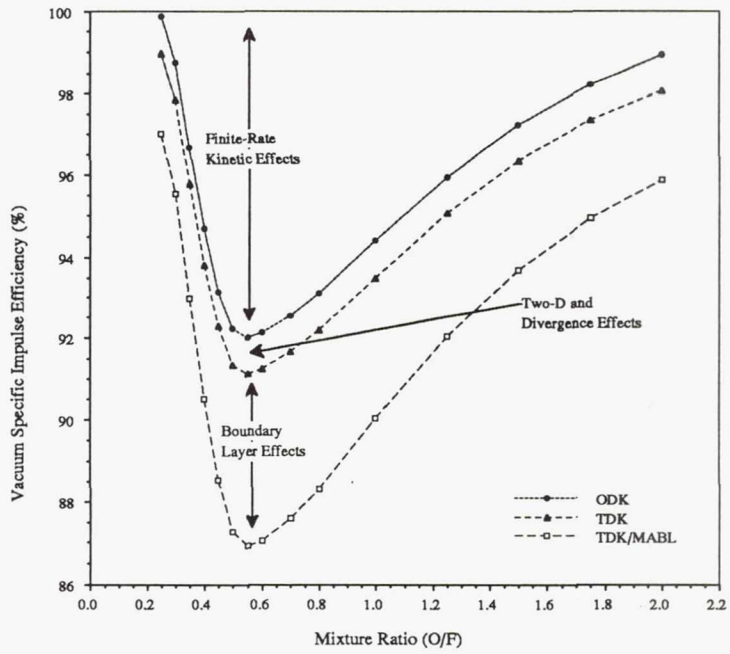

Figure 3. - Theoretical specific impulse efficiency for O2/CO in an RL10 rocket engine (referenced to ODE, Pc=1.4 MPa, Area Ratio=205, LCO regen. cooled)

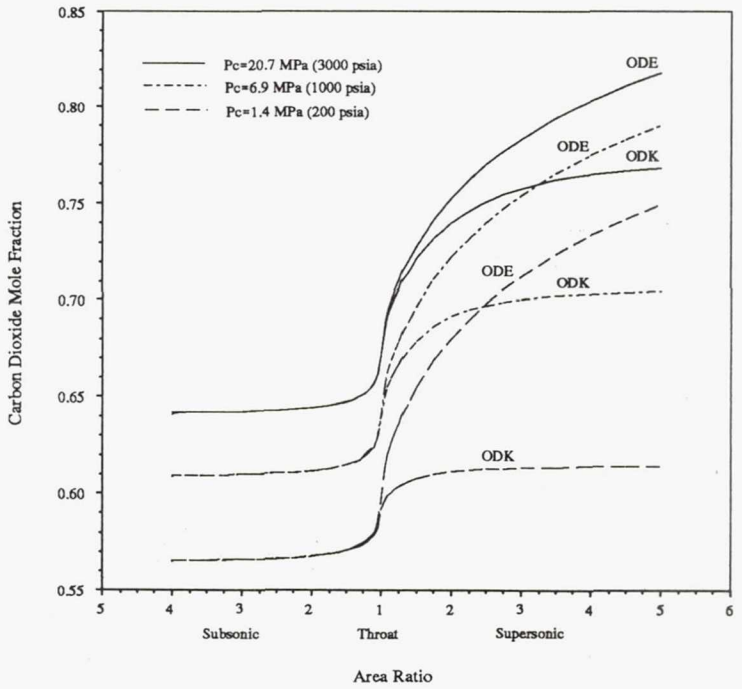

Figure 4. - Carbon dioxide recombination profiles assuming equilibrium and finite-rate chemistry for various chamber pressures (O/F=0.55)

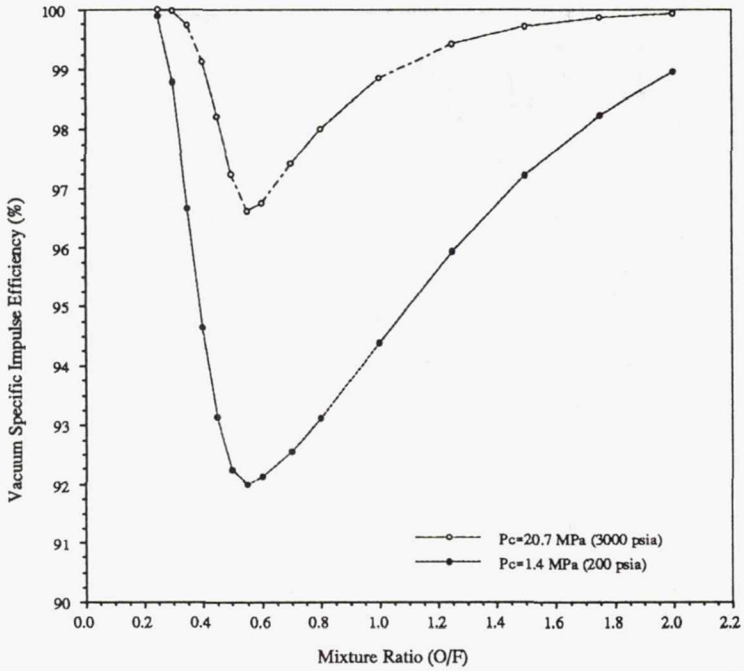

Figure 5. - Theoretical specific impulse efficiency assuming finite-rate kinetics for O2/CO in an RL10 rocket engine for different chamber pressures (Area Ratio=205, LCO regen. cooled)

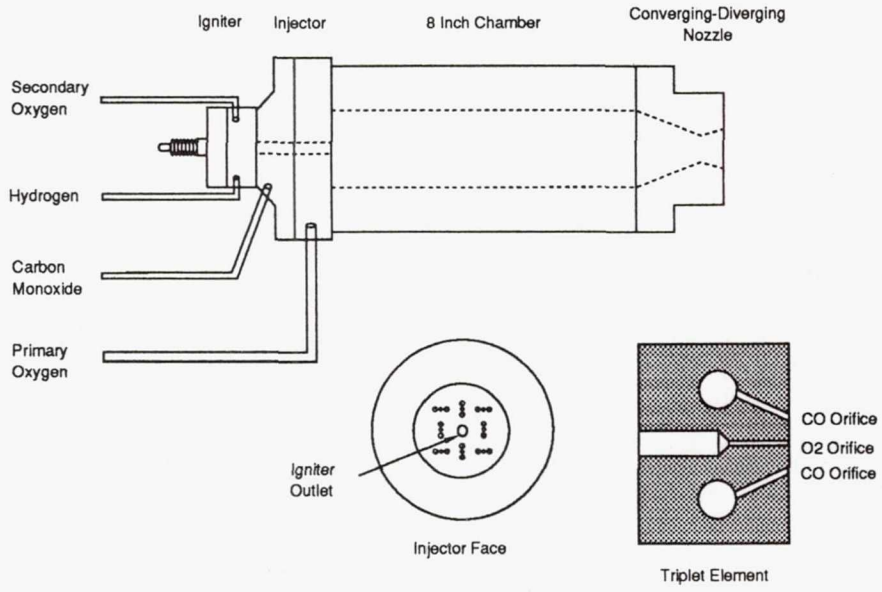

Figure 6. - O2/CO experimental test hardware schematic

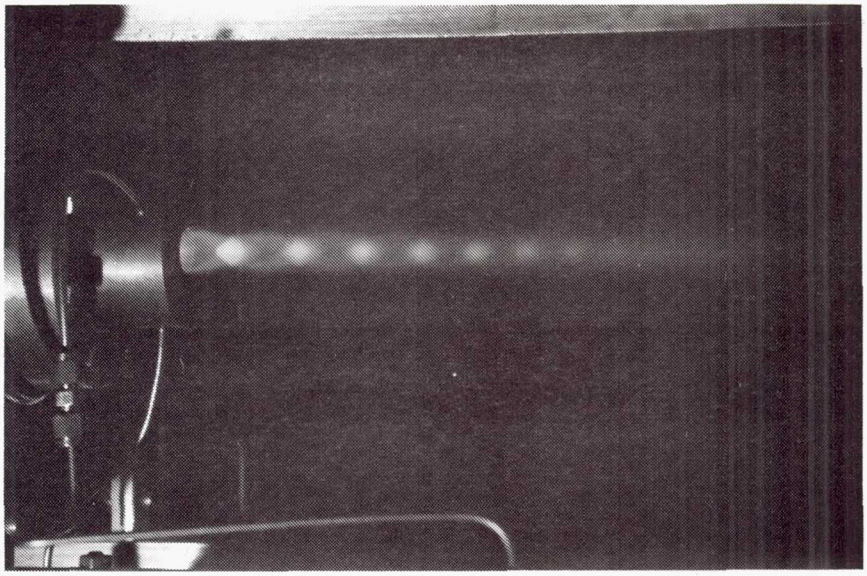

Figure 7. - Hot-fire of Carbon Monoxide and Oxygen.

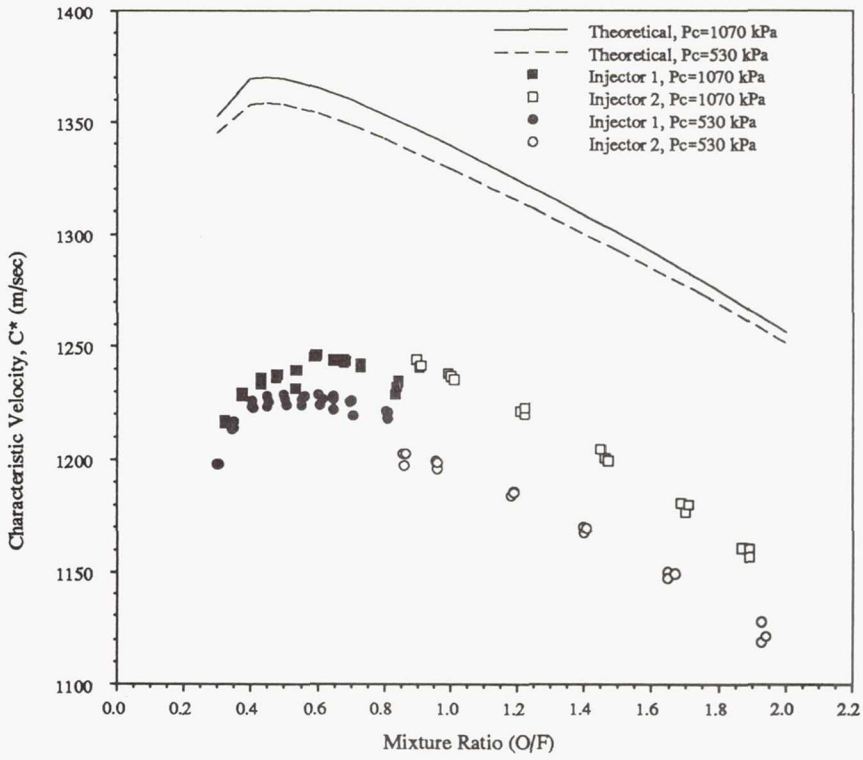

Figure 8. - O2/CO combustion experimental C* data

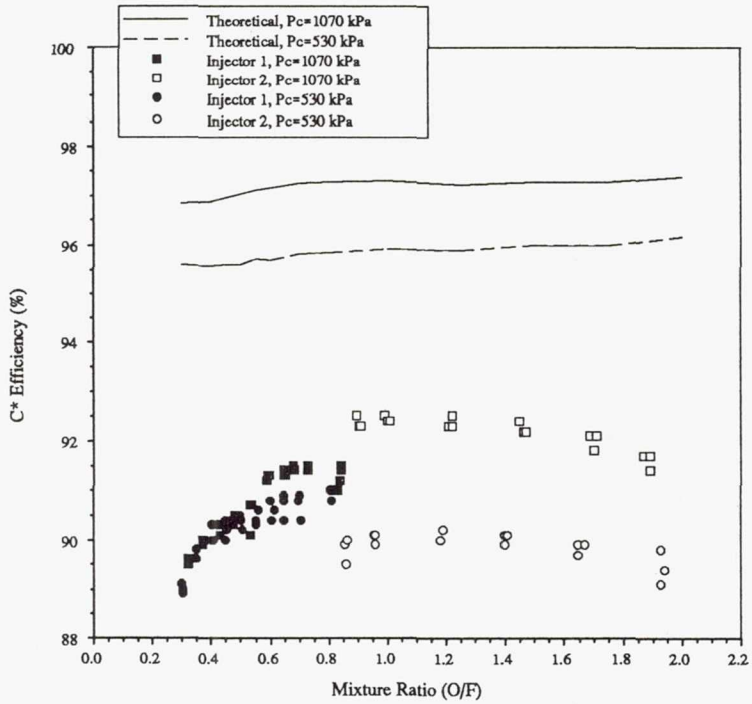

Figure 9. - O2/CO combustion experimental C* efficiency data (referenced to ODE)

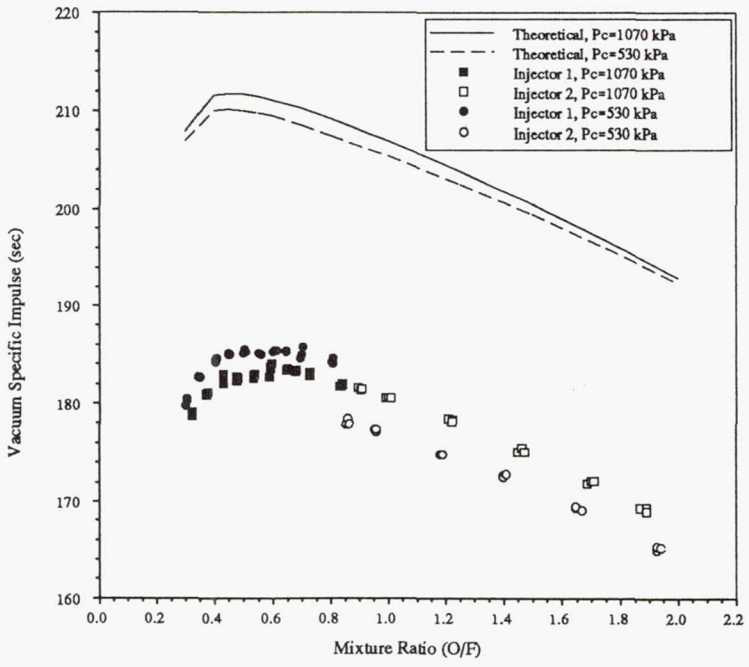

Figure 10. - O2/CO combustion experimental vacuum specific impulse data

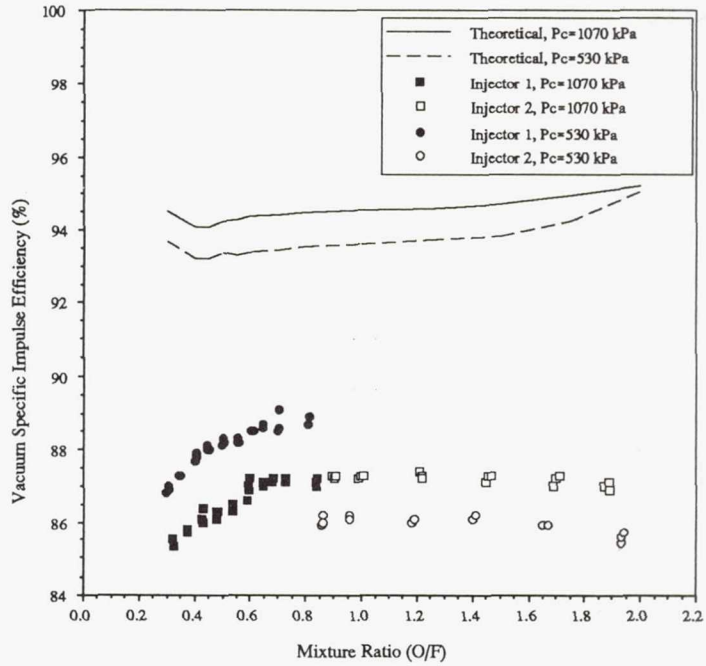

Figure 11. - O2/CO combustion experimental vacuum specific impulse efficiency data (referenced to ODE)

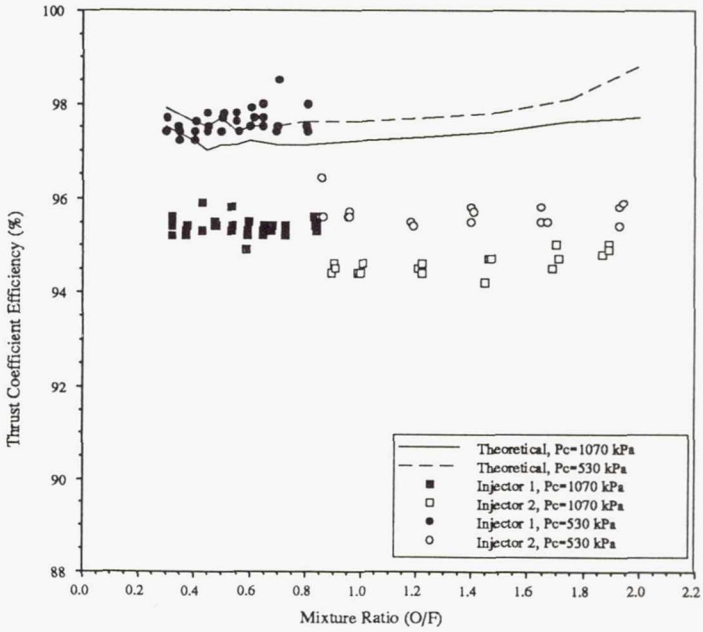

Figure 12. - Theoretical and experimental thrust coefficient efficiency for O2/CO tests (referenced to ODE)

NASA
National Aeronautics and Space Administration

Report Documentation Page

1. Report No.	2. Government Accession No.	3. Recipient's Catalog No.
NASA TM -104473 AIAA-91-2443		

4. Title and Subtitle
Carbon Monoxide and Oxygen Combustion Experiments: A Demonstration of Mars In Situ Propellants

5. Report Date

6. Performing Organization Code

7. Author(s)
Diane L. Linne

8. Performing Organization Report No.
E -6320

10. Work Unit No.
506 -42-72

9. Performing Organization Name and Address
National Aeronautics and Space Administration
Lewis Research Center
Cleveland, Ohio 44135 - 3191

11. Contract or Grant No.

13. Type of Report and Period Covered
Technical Memorandum

12. Sponsoring Agency Name and Address
National Aeronautics and Space Administration
Washington, D.C. 20546 - 0001

14. Sponsoring Agency Code

15. Supplementary Notes
Prepared for the 27th Joint Propulsion Conference cosponsored by AIAA, SAE, ASME, and ASEE, Sacramento, California, June 24-27, 1991. Responsible person, Diane L. Linne, (216) 433-2410.

16. Abstract
The feasibility of using carbon monoxide and oxygen as rocket propellants was examined both experimentally and theoretically. The steady-state combustion of carbon monoxide and oxygen was demonstrated for the first time in a subscale rocket engine. Measurements of experimental characteristic velocity, vacuum specific impulse, and thrust coefficient efficiency were obtained over a mixture ratio range of 0.30 to 2.0 and at chamber pressures of 1070 and 530 kPa (155 and 77 psia). The theoretical performance of the propellant combination was studied parametrically over the same mixture ratio range. In addition to one dimensional ideal performance predictions, various performance reduction mechanisms were also modeled, including finite-rate kinetic reactions, two-dimensional divergence effects, and viscous boundary layer effects.

17. Key Words (Suggested by Author(s))
Mars; Carbon monoxide; Combustion; Liquid propellant rocket engines; Extraterrestrial resources

18. Distribution Statement
Unclassified - Unlimited
Subject Categories 20 and 28

19. Security Classif. (of the report)	20. Security Classif. (of this page)	21. No. of pages	22. Price*
Unclassified	Unclassified	18	A03

*For sale by the National Technical Information Service, Springfield, Virginia 22161